International Journal of Modern Physics B
Vol. 35, No. 2 (2021) 2150027 (10 pages)

DOI: 10.1142/S0217979221500272

Effect of high bandgap AlAs quantum barrier on electronic and optical properties of $In_{0.70}Ga_{0.30}As/Al_{0.60}In_{0.40}As$ superlattice under applied electric field for laser and detector applications

B. O. Alaydin

Department of Physics, Institute for Quantum Electronics, ETH Zürich, 8093 Zürich, Switzerland
Department of Physics, Faculty of Science, Cumhuriyet University, 58140 Sivas, Turkey
balaydin@phys.ethz.ch

Received 17 July 2020
Revised 5 October 2020
Accepted 5 October 2020
Published 18 December 2020

Effect of high bandgap 0.5 nm AlAs on the electronic and optical properties of the $In_{0.70}Ga_{0.30}As/Al_{0.60}In_{0.40}As$ superlattice is investigated by using effective mass approximation under the electric field. Electronic transitions are obtained as 0.403 eV and 0.023 eV for E_{32} and E_{21} in the gain region. Thin AlAs increases electron confinement in the superlattice and prevents electron leakage in the gain region which mostly results in higher absorption/emission in the superlattice. AlAs has no major effects on transitions energies in the gain region but it is effectively decreasing the total absorption in the injector region and preventing the internal absorption. AlAs also makes the superlattice optically more stable by decreasing the high refractive index change in the injector region by factor 5.

Keywords: $In_{0.70}Ga_{0.30}As$ and $Al_{0.60}In_{0.40}As$; AlAs quantum barrier; superlattice; electric field; electronic and optical properties.

PACS numbers: 71.20.Mq, 42.70.Hj, 78.20.−e, 78.20.Ci, 61.50.Ah

1. Introduction

Nanoscale quantum mechanical systems have been very attractive since last couple of decades. One-dimensional quantum well (QW), two-dimensional quantum wire and three-dimensional quantum dot-based semiconductor hetero structures are studied extremely due to their crucial optical and electronic properties. The studies create a new field in condensed matter physics which results in lots of potential applications for optoelectronic devices such as high-speed electron optical modulators,[1] field-effect transistors,[2] infrared detectors[3] and semiconductor lasers.[4] Due

to the wide range of technological applications, hydrostatic pressure, temperature, electric field, magnetic field, laser field and different doping processes, etc. have been investigated deeply for single and multiple QWs.[5–9] The optical properties of low dimensional semiconductor systems have been widely examined in the last years.[10–18] Radu[12] analyzed the laser-dressing of electronic quantum states in graded semiconductor structure. Karimi and Vafaei[13] projected the light on the optical rectification in a strained InGaN/AlGaN QW in case of effect of the spontaneous and piezoelectric polarization fields on the potential profile. Also, they did research on the second harmonic generation. Zeiri *et al.*[14] explored inter-subband (ISB) resonant enhancement of the nonlinear optical properties in asymmetric (CdS/ZnSe)/X-BeTe-based QWs. Keshavarz and Karimi studied linear and nonlinear ISB optical absorption in symmetric double semi-parabolic QW. Rodriguez *et al.* calculated refractive index change and optical absorption coefficients for n-doped QW.[16] As a result, all the mentioned studies in these papers are not considered owing to their geometrical differences, there have also been crucial effects on the optical properties of semiconductor structures. However, even though there have been many papers in the literature about optical properties of multi QW, optical properties of superlattices (SL) are not investigated broadly due to complexity of structures and numerical difficulties.

Since 1990, SL have been really attractive due to their important electronic properties, optical properties and possible practical applications in semiconductor device technology.[19–22] Sirtori *et al.*[23] grew superlattice by using molecular-beam epitaxy and they study lasing performance of quantum cascade lasers (QCLs). Razeghi *et al.*[24] focused on SL in the framework of different band alignments to compare the results with the experimental data and Shi *et al.* calculated the linear and nonlinear optical absorption coefficients in superlattice under electric field.[25]

In this study, two superlattice structures (gain and injector regions) are studied under applied electric field. Electronic and optical properties of $In_{0.70}Ga_{0.30}As/Al_{0.60}In_{0.40}As$ SL are examined depending on the barrier height. Thin AlAs layer (0.5 nm) is placed in the middle of barriers of the injector region to increase barrier height and confinement of electrons in the wells. ISB transition energies, dipole matrix elements, linear absorption coefficients, nonlinear absorption coefficients, linear refractive index changes and nonlinear refractive index changes are found out numerically for E_{21}, E_{32} and E_{43} transitions. For numerical calculations, effective mass approximation is used and time-independent Schrödinger equation is solved by using finite difference method.

2. Theory

In this work, $In_{0.70}Ga_{0.30}As/Al_{0.60}In_{0.40}As$ SL grown in z-direction is studied. SLs are separated as gain and injector regions and Schrödinger equations are solved independently due to noninteraction of the quantum energy levels under effective mass approximation. Electric field is chosen in the growth direction as $\mathbf{F} = F\mathbf{z}$.

Hamiltonian in this case can be written as[26]

$$H = \frac{\mathbf{p}^2}{2m^*} + V(z) + eF\mathbf{z}, \tag{1}$$

where m^* is the effective mass of electron and in this study, it is taken as $0.07927m_0$. m_0 is the free electron mass, $\mathbf{p}^2$ is the electron momentum operator, e is the electron charge and $V(z)$ is the confinement potential. Conduction band offset and potential discontinuity $V(z)$ are taken as 731 meV (1.8060 eV for AlAs barrier) and 0.6 for $In_{0.70}Ga_{0.30}As/Al_{0.60}In_{0.40}As$ SL system. Eigenfunctions of the infinite potential well are used for well width L to solve the following equation:

$$\psi_n(z) = \sqrt{\frac{2}{L}} \cos\left(\frac{n\pi z}{L}\right) - \delta n, \tag{2}$$

where δn is

$$\delta n = \begin{cases} 0, & n \text{ is odd}, \\ \dfrac{\pi}{2}, & n \text{ is even}. \end{cases} \tag{3}$$

After obtaining the energy levels and wave functions, linear and nonlinear absorption coefficient is calculated as follows[27]:

$$\beta^{(1)}(w) = w\sqrt{\frac{\mu}{\varepsilon_r}} \frac{|M_{ij}|^2 \sigma_v \hbar\Gamma_{ij}}{\left(\Delta E_{ij} - \hbar w\right)^2 + \left(\hbar\Gamma_{ij}\right)^2} \tag{4}$$

$$i\beta^{(3)}(w) = -2w\sqrt{\frac{\mu}{\varepsilon_r}} \left(\frac{I}{\varepsilon_0 n_r c}\right) \frac{|M_{ij}|^4 \sigma_v \hbar\Gamma_{ij}}{\left(\left(\Delta E_{ij} - \hbar w\right)^2 + (\hbar\Gamma_{ij})^2\right)^2} \times \left(1 - \frac{|M_{ff} - M_{ii}|}{|2M_{ii}|^2} \frac{(\Delta E_{ij} - \hbar w)^2 - (\hbar\Gamma_{ij})^2 + 2\Delta E_{ij}(\Delta E_{ij} - \hbar w)}{\Delta E_{ij}^2 + (\hbar\Gamma_{ij})^2}\right), \tag{5}$$

where w is the angular frequency, Γ_{ij} is the ISB relaxation time, μ is the magnetic permeability, ε_r is the real part of the electrical permittivity, σ_v is the carrier number, $\hbar$ is the reduced Planck constant and ΔE_{ij} is the energy difference between final and initial energy levels of the electron. M_{ij} is the dipole matrix element and it is defined as[28]

$$M_{ij} = \int \psi_f(z)^* |e| z \psi_i(z) dz. \tag{6}$$

Then total absorption coefficient is given as

$$\beta(w) = \beta^{(1)}(w) + \beta^{(3)}(w). \tag{7}$$

The linear and nonlinear refractive index change is expressed as[29]

$$\frac{\Delta n^{(1)}(w)}{n_r} = \frac{|M_{ij}|^2 \sigma_v}{2n_r^2 \varepsilon_0} \left[\frac{\Delta E_{ij} - \hbar w}{\left(\Delta E_{ij} - \hbar w\right)^2 + \left(\hbar\Gamma_{ij}\right)^2}\right], \tag{8}$$

$$\frac{\Delta n^{(3)}(w)}{n_r} = -\frac{\mu c|M_{ij}|^2}{4n_r^3\varepsilon_0}\frac{\sigma_v I}{((\Delta E_{ij}-\hbar w)^2+(\hbar\Gamma_{ij})^2)^2}\Big[4(\Delta E_{ij}-\hbar w)|M_{ij}|^2 - \frac{(M_{ff}-M_{ii})^2}{\Delta E_{ij}^2+(\hbar\Gamma_{ij})^2}\{(\Delta E_{ij}-\hbar w)\Delta E_{ij}(\Delta E_{ij}-\hbar w) - (\hbar\Gamma_{ij})^2(2\Delta E_{ij}-\hbar w)\}\Big]. \tag{9}$$

Finally, total refractive index change is given as

$$\frac{\Delta n(w)}{n_r} = \frac{\Delta n^{(1)}(w)}{n_r} + \frac{\Delta n^{(3)}(w)}{n_r}. \tag{10}$$

3. Result and Discussion

The parameters used in the study are as follows: $m^* = 0.07927m_0$, $V_0 = 731$ meV, $I = 0.4\frac{MW}{\text{cm}^2}$, $\mu = 4\pi \times 10^{-7}$ Hm^{-1}, $\sigma_v = 2.5 \times 10^{17}$ cm^{-3}, $\tau_{21} = 0.3$ ps, $\tau_{32} = 2.8$ ps $\Gamma_{ij} = \frac{1}{\tau_{ij}}$, and $n_r = 3.0936$. In this study, electronic and optical properties of two superlattice structures are compared under applied electric field. Conduction band diagram of both structures is shown in Fig. 1.

Thickness of structures is as follows for low barrier and high barrier SL: 2.0/**1.8**/1.8/**1.8**/1.9/**1.8**/1.5/**2.0**/1.5/**2.3**/1.4/**2.5**/1.3/**3.0**/1.3/**3.4**/1.2/**3.6**/1.1/**4.5**/0.5/**1.2**/3.5/**2.3**/3.0/**2.8**. Low barrier SL is the same structure of reference.[30] 0.5 nm AlAs barrier inserted in the middle of the normal $Al_{0.60}In_{0.40}As$ barrier by keeping total barrier thickness the same. QWs are in normal font, quantum barriers are bold and AlAs layers are bold and underlined.

In case of absence of electric field [Fig. 1(a)], ground and first excited states are localized in middle and right QW in the gain region. Localization of second excited state is distributed between left and middle QW. While third excited state is distributed mostly in right QW in gain region and there is also some portion of that around left QW in gain region. Energy of the third excited state is also similar to barrier height so it is like almost unbounded energy state. In the meantime, all energy states are distributed in the wells (mostly in the left wells without localizing in one well) in injector regions. After applying electric field, ground and first excited energy states switch their localization in the wells and first and second excited states are localized in the middle QW under applied electric field [Fig. 1(b)] in the gain region. There is almost no localization in the first QW because this well is used to adjust energy levels of states in the superlattice by changing the thickness. Also, as an effect of electric field, third excited state localizes in the right QW completely. After applying electric field and placing thin AlAs high bandgap material in injector region [Fig. 1(c)], localization of the energy states occurs mainly in the one well and localization is shifting to right wells. As expected, energies of all states are increasing as a result of higher barrier height. Energy states, transition energies and

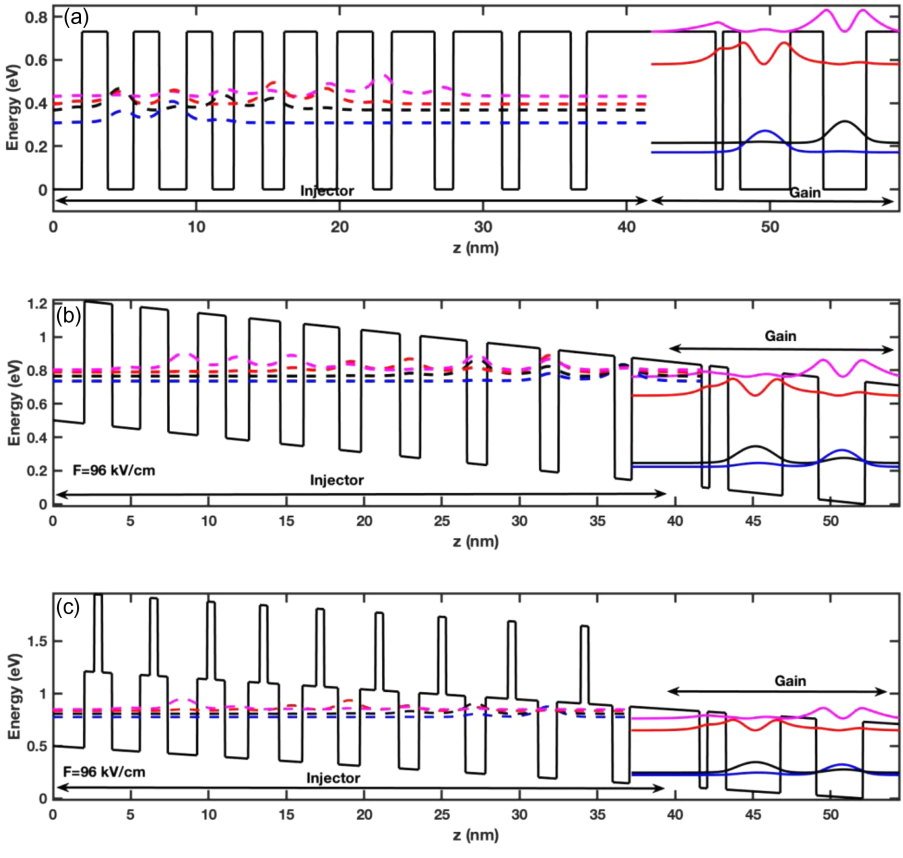

Fig. 1. (Color online) Conduction band diagram of one period $In_{0.70}Ga_{0.30}As/Al_{0.60}In_{0.40}As$ SL. (a) low barrier zero electric field (b) low barrier structure under 96 kV/cm applied electric field and (c) high barrier structure with 0.5 nm AlAs under applied 96 kV/cm applied electric field. Solid lines are energy levels of gain region and dashed lines are energy levels of injector region.

square of dipole matrix are given in Table 1. Addition of high bandgap AlAs has no major effect on the transition energies in the gain region because of noninteraction between gain and injector regions.

In the gain region, third excited state is like unbounded energy state due to low barrier height and that causes electron leakage in the structure under electric field. However, inserting high bandgap AlAs quantum barrier confines the third excited state in the gain region and prevent electron leakage under applied electric field. That is important to have high emission/absorption from the structure. On the other hand, AlAs barriers change distribution of electron in the injector region also. Localization mostly happens in one well while it is distributed between wells in low barrier structure. It is important to provide electron injection from ground state of injector region to the second excited state of gain region for laser and detector applications.

Table 1. Energy states, transition energies and square of dipole matrix element for gain, injector and injector region with AlAs barrier.

Energy states and square of dipole matrix elements	Gain	Injector	Injector with AlAs
E_1 (eV)	0.2234	0.5120	0.5519
E_2 (eV)	0.2461	0.5419	0.5833
E_3 (eV)	0.6491	0.5663	0.6116
E_4 (eV)	0.7620	0.5794	0.6253
ΔE_{12} (eV)	0.0227	0.0298	0.0314
ΔE_{23} (eV)	0.4030	0.0244	0.0282
$\lvert\langle\psi_2\lvert\psi_1\rangle\rvert^2 \times 10^{-18}$	5.0653	7.2545	4.7685
$\lvert\langle\psi_3\lvert\psi_2\rangle\rvert^2 \times 10^{-18}$	1.3840	1.3519	4.9394

First and second excited states are localized in the second QW under applied electric field in the gain region and transition energy is $E_{32} = 403$ meV which correspond to emission/absorption in middle infrared region. Energy of all states in the injector region is higher than second excited state of the gain region, that is suitable band alignment for electron flow from injector to gain region. In case of cascaded growth of active region, one electron can contribute many radiative transition/emissions as like in QCLs and detectors.

In this part of paper, optical properties are discussed. Figure 2 shows linear absorption coefficient change of E_{21} and E_{32} transitions for gain, injector and injector with AlAs regions.

Absorption of the middle infrared light is strong in the gain region for E_{32} however absorption coefficient of E_{21} is not comparable to E_{32}. In the injector region very strong absorption occurs at lower energy for E_{21} and E_{32}. E_{32} is much stronger than E_{21}. That can cause strong absorption of radiative emission obtained in the gain. As similar absorption of E_{32} is stronger than E_{21} in the AlAs inserted injector region, absorption coefficient is reduced one-third as an effect of high bandgap AlAs layer and that is good to prevent internal absorption in the structure.

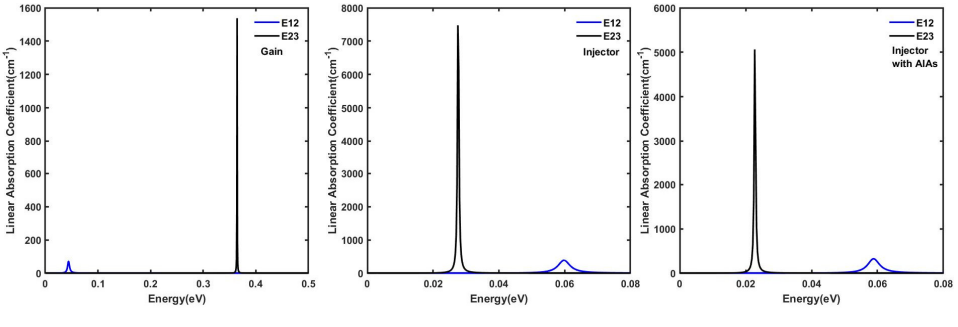

Fig. 2. (Color online) Energy versus linear absorption coefficient change of gain, injector and injector with AlAs regions.

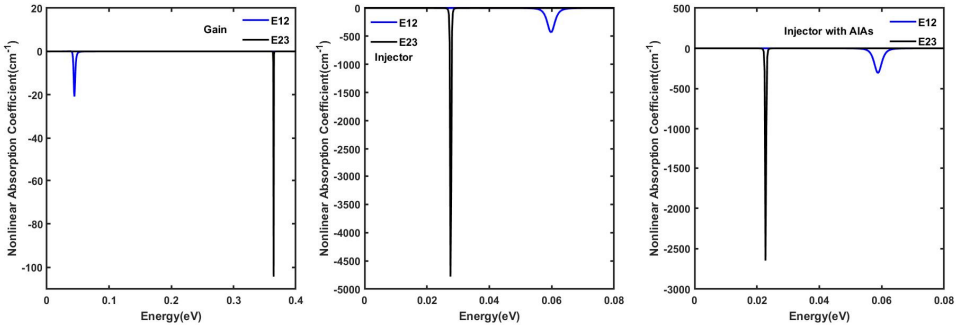

Fig. 3. (Color online) Energy versus linear absorption coefficient change of gain, injector and injector with AlAs regions.

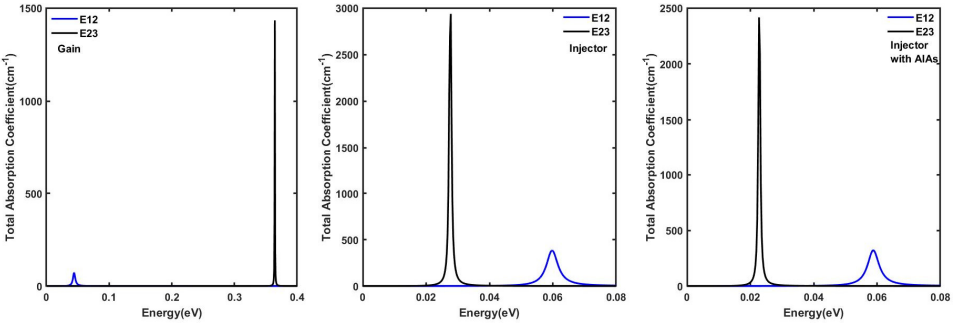

Fig. 4. (Color online) Energy versus total absorption coefficient change of gain, injector and injector with AlAs regions.

Figure 3 shows nonlinear absorption coefficients, nonlinear absorption is very sharp and strong for E_{32} transition in the gain region and E_{21} is factor 5 is less but nonlinear absorption is less pronounced due to low doping in the gain region. In the injector region, E_{32} is stronger and E_{21} is factor 10 less than E_{32}. Nonlinear absorption coefficient is almost half when AlAs is placed in the barrier as desired. Also, absorption energies have slightly blueshifts.

In the end, total absorption coefficients are calculated for all regions. Nonlinear absorption decreases negligible due to low doping density in this region. Nonlinear effect is dominant for the injector region, especially for E_{32}, but after adding high bandgap AlAs, nonlinear effects becomes less important. Absorption in the injector region decreases for E_{32} and E_{21} so that E_{32} is obviously stronger in this region.

Linear refractive index change in the gain region for E_{32} is relatively low and it is lower for E_{21} transition. E_{32} is sharper than E_{21} due to stronger dipole matrix element. Linear refractive index change in the injector region is strong for E_{32} but it is negligible for E_{21}. Linear refractive index change of injector region with AlAs is a bit sharper otherwise high bandgap AlAs barrier has no major effect on linear refractive index change owing to similar dipole matrix element value.

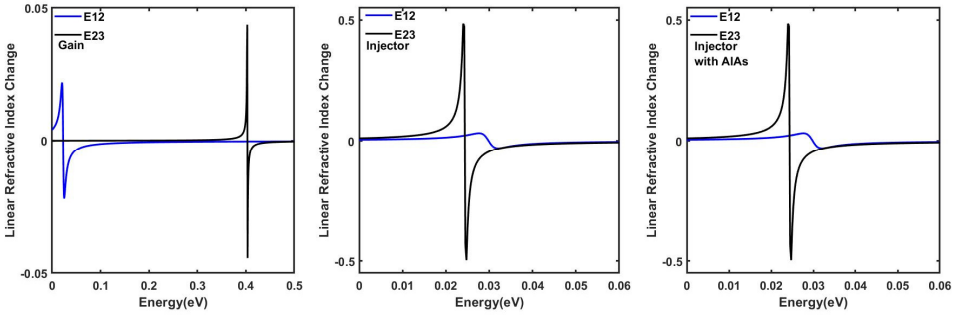

Fig. 5. (Color online) Energy versus linear refractive index change of gain, injector and injector with AlAs regions.

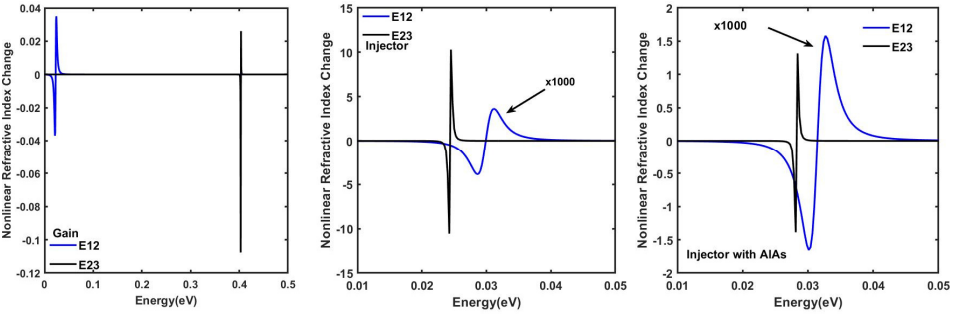

Fig. 6. (Color online) Energy versus nonlinear refractive index change of gain, injector and injector with AlAs regions.

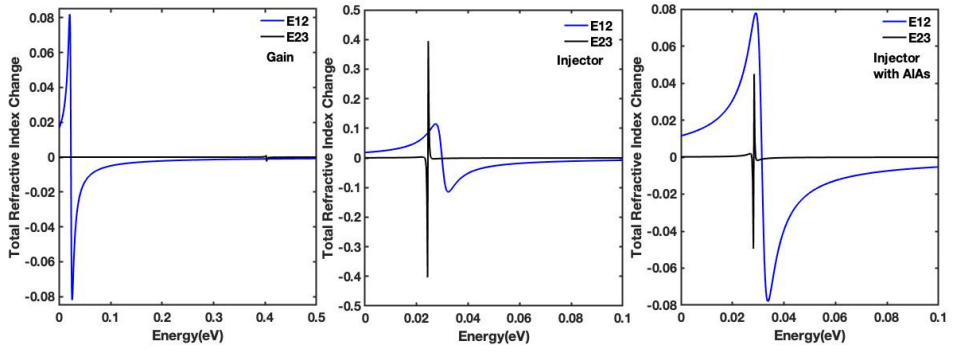

Fig. 7. (Color online) Energy versus total refractive index change of gain, injector and injector with AlAs regions.

Nonlinear refractive index change occurs at transition energy of the E_{32} in the gain region and in the negative direction it is higher. Nonlinear effects are not changing refractive index effectively for E_{21}. In the injector region, nonlinear effects have really high impact on the refractive index change for E_{32} but it is negligible for

E_{21}. Adding high bandgap AlAs decreasing nonlinear effect due to high bandgap and superlattice becomes optically more stable without causing major increase in refractive index change for E_{21}.

In the end, nonlinear effects balance refractive index change for E_{32} transition and change is really low in the gain region. In the injector region, it is also balancing high refractive index change but change is still too much to have stable superlattice. High bandgap AlAs makes the injector region certainly much more stable. Nonlinear properties of superlattice are dominant and decreasing refractive index change.

4. Conclusion

As a summary, effect of addition of high bandgap AlAs is studied on the electronic and optical properties of $In_{0.70}Ga_{0.30}As/Al_{0.60}In_{0.40}As$ superlattice. Calculations are done by using finite difference method to obtain wave functions and energy states under effective mass approximation. 0.5 nm AlAs high bandgap barrier provides higher confinement in the gain region without changing transition energies and higher confinement results in lower electron leakage. Linear, nonlinear and total absorption coefficients show that high absorption occurs in the gain and injector region. Unwanted internal absorption in the gain region decreases with addition of AlAs so that low absorption happens in the injector region. It is found that refractive index change is very weak in the gain region however it is very high in the injector region, which is also compensated by thin AlAs barrier and nonlinear effects in the superlattice. As a conclusion, this study is exceptional due to considered effect and can contribute to literature while designing superlattice based devices.

References

1. A. D. Yoffe, *Adv. Phys.* **50**, 1 (2001).
2. M. Vali, D. Dideban and N. Moezi, *Physica E* **69**, 360 (2015).
3. D. M. T. Kuo, A. Fang and Y. C. Chang, *Infrared Phys. Technol.* **42**, 433 (2001).
4. J. Zheng *et al.*, *Opt. Laser Technol.* **67**, 38 (2015).
5. I. Karabulut, M. E. Mora-Ramos and C. A. Duque, *J. Lumin.* **131**, 1502 (2011).
6. J. C. Martinez-Orozco, M. E. Mora-Ramos and C. A. Duque, *J. Lumin.* **132**, 449 (2012).
7. H. Dakhlaoui, S. Almansour and E. Algrafy, *Superlattices Microstruct.* **77**, 196 (2015).
8. V. V. Tai and N. Q. Khanh, *Physica E* **67**, 84 (2015).
9. E. C. Niculescu, N. Eseanu and A. Radu, *Opt. Commun.* **294**, 276 (2013).
10. B. O. Alaydin *et al.*, *Int. J. Mod. Phys. B* **33**, 1950054 (2019).
11. B. O. Alaydin, E. Ozturk and S. Elagoz, *Int. J. Mod. Phys. B* **32**, 5 (2018).
12. A. Radu, *Solid State Commun.* **157**, 11 (2013).
13. M. J. Karimi and H. Vafaei, *Superlattices Microstruct.* **78**, 1 (2015).
14. N. Zeiri *et al.*, *Opt. Mater.* **35**, 875 (2013).
15. A. Keshavarz and M. Karimi, *Phys. Lett. A* **374**, 2675 (2010).
16. K. Rodriguez-Magdaleno *et al.*, *J. Lumin.* **147**, 77 (2014).
17. G. Safarpour *et al.*, *Superlattices Microstruct.* **75**, 936 (2014).

18. C. A. Duque *et al.*, *J. Lumin.* **154**, 559 (2014).
19. S. Nagahama *et al.*, *Jpn. J. Appl. Phys.* **39**, L647 (2000).
20. D. Li *et al.*, *Adv. Mater.* **24**, 845 (2012).
21. Y. Bai *et al.*, *Appl. Phys. Lett.* **97**, 251104 (2010).
22. A. Evans *et al.*, *Appl. Phys. Lett.* **85**, 2166 (2004).
23. C. Sirtori *et al.*, *Appl. Phys. Lett.* **73**, 3486 (1998).
24. M. Razeghi and B. Nguyen, *Phys. Procedia* **3**, 1207 (2003).
25. J. Shi and S. Pan, *Superlattices Microstruct.* **17**, 1 (1995).
26. I. Karabulut and C. A. Duque, *Physica E* **43**, 1405 (2011).
27. B. Chen *et al.*, *Solid State Commun.* **149**, 310 (2009).
28. L. Zhang *et al.*, *Superlattices Microstruct.* **48**, 434 (2010).
29. M. Gambhir *et al.*, *J. Lumin.* **143**, 361 (2013).
30. J. Faist *et al.*, *Appl. Phys. Lett.* **72**, 680 (1998).